The Journal of Neuroscience, November 15, 2000, 20(22):8462–8473

Origins and Distribution of Cholinergically Induced β Rhythms in Hippocampal Slices

Ken Shimono,[1] Fernando Brucher,[2] Richard Granger,[2] Gary Lynch,[3] and Makoto Taketani[1]

[1]*Technology Development Center, Panasonic, Cypress, California 90630, and Departments of* [2]*Information and Computer Science and* [3]*Psychiatry and Human Behavior, University of California, Irvine, California 92697*

Regional variations and substrates of high-frequency rhythmic activity induced by cholinergic stimulation were studied in hippocampal slices with 64-electrode recording arrays. (1) Carbachol triggered β waves (17.6 ± 5.7 Hz) in pyramidal regions of 75% of the slices. (2) The waves had phase shifts across the cell body layers and were substantially larger in the apical dendrites than in cell body layers or basal dendrites. (3) Continuous, two-dimensional current source density analyses indicated apical sinks associated with basal sources, lasting ~10 msec, followed by apical sources and basal sinks, lasting ~20 msec, in a repeating pattern with a period in the range of 15–25 Hz. (4) Carbachol-induced β waves in the hippocampus were accompanied by 40 Hz (γ) oscillations in deep layers of the entorhinal cortex. (5) Cholinergically elicited β and γ rhythms were eliminated by antagonists of either AMPA or GABA receptors. Benzodiazepines markedly enhanced β activity and sometimes introduced a distinct γ frequency peak. (6) Twenty Hertz activity after orthodromic activation of field CA3 was distributed in the same manner as carbachol-induced β waves and was generated by a current source in the apical dendrites of CA3. This source was eliminated by high concentrations of $GABA_A$ receptor blockers. It is concluded that cholinergically driven β rhythms arise independently in hippocampal subfields from oscillatory circuits involving (1) bursts of pyramidal cell discharges, (2) activation of a subset of feedback interneurons that project apically, and (3) production of a $GABA_A$-mediated hyperpolarization in the outer portions of the apical dendrites of pyramidal neurons.

Key words: current source density; β rhythm; acetylcholine; hippocampus; multielectrode array; γ rhythm

Rhythmic activity in the hippocampus of small mammals is described as falling into three frequency bands: 4–10 Hz (θ), 10–30 Hz (β), and >30 Hz (γ) (for a recent discussion, see Traub et al., 1998, 1999). θ is by far the best studied of these and is generally agreed to be related to, among other things, locomotor activity (Vanderwolf, 1969) and memory encoding (Landfield et al., 1972; Vertes and Kocsis, 1997). In accord with the latter idea is the close relationship between θ and long-term potentiation (Larson and Lynch, 1986; Larson et al., 1986, 1993), a probable substrate of certain forms of memory. The functional correlates of the higher frequency rhythms have recently become the subjects of considerable interest. γ Activity was first analyzed in the olfactory system (for an early review, see Freeman, 1975) with the conclusion that it allows coherence to develop between the bulb, piriform cortex, and entorhinal cortex before the arrival of an odor (Kay and Freeman, 1998). Activity falling in the γ range also appears in the visual cortex during cue presentation (Gray and Singer, 1989) where it is proposed to transiently synchronize cells with disparate receptive fields. Synchronization, according to this hypothesis, allows multiple features of a cue to be assembled into a coherent representation (for review, see Singer, 1998). β Rhythms have not typically been discriminated from the γ wave in discussions of high-frequency hippocampal activity although they have been selectively induced in hippocampal slices (Boddeke et al., 1997). In any event, the growing evidence that high-frequency synchronization is essential to coherent operations in the cortical telencephalon has emphasized the importance of identifying the pathways and transmitters responsible for the β and γ oscillations.

Ascending cholinergic projections promote endogenous oscillations including those in the β and γ ranges. Although early work (Stumpf, 1965) found cholinergic blockers or septal lesions to be without obvious effect, subsequent studies showed that fast waves (30–60 Hz) in freely moving rats are enhanced by the cholinesterase inhibitor physostigmine and substantially reduced by antagonists (Leung, 1985). Cholinergic stimulation of hippocampal or entorhinal slices is usually described as inducing seconds-long episodes of θ-like activity (Konopacki et al., 1987; MacVicar and Tse, 1989; Dickson and Alonso, 1997; Williams and Kauer, 1997), but recent experiments show that it can also trigger higher frequency rhythms (20–40 Hz) in cortical and hippocampal slices (Boddeke et al., 1997; Fisahn et al., 1998). Cholinergic septohippocampal fibers innervate discrete regions of the hippocampal system (Lewis and Shute, 1967; Mosko et al., 1973; Frotscher and Leranth, 1985; Matthews et al., 1987) where they contact subpopulations of interneurons and select dendritic zones of principal cells (Mosko et al., 1973; Lynch et al., 1978; Matthews et al., 1987). Stimulation of muscarinic receptors depolarizes pyramidal cells, depresses release from some interneurons, and increases the excitability of others (Pitler and Alger, 1992; Behrends and Bruggencate, 1993). The combination of *in vivo* and *in vitro* results suggests that acetylcholine plays an important role in generating high-frequency synchronous activity in the cortical telencephalon.

How cholinergically driven high-frequency rhythms affect cortical operations depends on whether they are regionally specialized and how they are produced. Carbachol-elicited oscillations are reported to originate in restricted loci in the entorhinal cortex (Dickson and Alonso, 1997) and hippocampus (Fisahn et al., 1998), but a more general answer requires systematic mapping over broad expanses of the entorhinohippocampal system. The present studies made use of a recently introduced device (Oka et al., 1999) for simultaneously recording from 64 sites to address the origins and regional variations in cholinergically induced high-frequency rhythms in the hippocampal region.

MATERIALS AND METHODS

Preparation of multielectrode array. Procedures for the preparation of the recently introduced Multi-Electrode Dish (Panasonic; MED probe) are described by Oka et al. (1999). The device has an array of 64 planar

Received Feb. 16, 2000; revised Aug. 23, 2000; accepted Aug. 29, 2000.

This work was supported in part by Grants N00014-98-1-0825 and N00014-98-1-0609 from the Defense Advanced Research Projects Agency and the Office of Naval Research. We thank Cheryl Cotman for her assistance with the current source density color maps and Laura Colgin for helpful discussions.

Correspondence should be addressed to Dr. Gary Lynch, Psychiatry Department, University of California, Irvine, CA 92697. E-mail: glynch@uci.edu.

 0270-6474/00/208462-12$15.00/0

microelectrodes, each having a size of 50 × 50 μm, arranged in an 8 × 8 pattern. Probes come with two types of interpolar distance, 150 μm (Panasonic; MED-P515AP) and 450 μm (Panasonic; MED-P545AP).

For sufficient adhesion of the slice to the probe, the surface of the MED probe was treated with 0.1% polyethylenimine (Sigma, St. Louis, MO; P-3143) in 25 mM borate buffer, pH 8.4, for 8 hr at room temperature. The probe surface was rinsed three times with sterile distilled water. The probe (chamber) was then filled with DMEM and F-12 mixed medium, containing 10% fetal bovine serum (Life Technologies, Gaithersburg, MD; 16141-079) and 10% horse serum (Life Technologies; 16050-122), for at least 1 hr at 37°C. DMEM and F-12 mixed medium is a 1:1 mixture of DMEM and Ham's F-12 (Life Technologies; D/F-12 medium, 12400-024), supplemented with N_2 supplement (Life Technologies; 17502-014) and hydrocortisone (20 nM; Sigma; H0888).

Preparation of hippocampal slices. A 17- to 24-d-old Sprague Dawley rat was killed by decapitation after anesthesia with halothane (2-bromo-2-chloro-1,1,1-trifluoroethane; Sigma; B4388), and the whole brain was removed carefully. The brain was immediately soaked for ~2 min in ice-cold, oxygenated preparation buffer of the following composition (in mM): 124 NaCl, 26 $NaHCO_3$, 10 glucose, 3 KCl, 1.25 NaH_2PO_4, 2 $CaCl_2$, and 2 $MgSO_4$. Appropriate portions of the brain were trimmed and placed on the ice-cold stage of a vibrating tissue slicer (Leica, Nussloch, Germany; VT-1000S). The stage was immediately filled with both oxygenated and frozen preparation buffers. The thickness of each tissue slice was 350 μm. Each slice was gently taken off the blade by a painting brush, trimmed, and immediately soaked in the oxygenated preparation buffer for 1 hr at room temperature. Then a slice was placed on the center of the MED probe. The slice was positioned to cover the 8 × 8 array. After positioning the slice, the MED probe was immediately placed in a box filled with 95% O_2 and 5% CO_2 and allowed to recover at 32°C for 1 hr.

Electrophysiological recording. During electrophysiological recording, the slices on the MED probe were placed in a small CO_2 incubator (Asahi Lifescience; model 4020) at 32°C. After recovery of the slice on the MED probe, the medium was replaced with DMEM and F-12 mixed medium without serum. The slices were on the interface, and a moisturized 95% O_2 and 5% CO_2 gas mixture was blown from above. In this condition, the responses were recorded for >2 hr.

Drugs were purchased from Research Biochemicals (Natick, MA; diazepam, bicuculline, CNQX, and 2-hydroxysaclofen) or Sigma (all other compounds). All drugs were bath applied at known concentrations and were prepared daily from frozen aliquots.

Spontaneous and evoked field potentials at all 64 sites were recorded simultaneously with the multichannel recording system (Panasonic; MED64 system) at a 20 kHz sampling rate. In the case of the evoked response, one of the planar microelectrodes out of the 64 available was used for the stimulating cathode. Bipolar constant-current pulses (10–50 μA; 0.1 msec) were produced by the data acquisition software via the isolator. The stimulating microelectrode was selected by the 64-switch box.

Current source density analysis. The well studied methods of current source density (CSD) analysis use the Laplacian transform (∇^2) on measured field potentials (ϕ) to attempt to identify the locations and relative magnitudes of current sources and sinks (I_m) (for review, see Howland et al., 1955; Mitzdorf, 1985):

$$I_m = -(\sigma_x \nabla_x^2 \phi + \sigma_y \nabla_y^2 \phi + \sigma_z \nabla_z^2 \phi),$$

where σ is the conductivity in each of the three orthogonal dimensions. The method is rarely used in its full three-dimensional form for electrophysiological measures (Nicholson, 1973; Nicholson and Freeman, 1975; Nicholson and Llinas, 1975), but rather a reduced form in one dimension is typically applied (Haberly and Shepherd, 1973; Ketchum and Haberly, 1993; Kolta et al., 1996). One-dimensional current source density analyses are, however, conducted in material of two or more dimensions (e.g., a brain slice), with the consequence that any currents occurring orthogonally to the axis of measure are undetected and the resulting one-dimensional results may therefore be misleading. Care is thus taken in one-dimensional analyses to ascertain that there are at most minimal currents occurring laterally to the orientation in which samples are measured. This is done typically by aligning the linear series of measures to be parallel to the direction of apical dendritic growth, because it has been demonstrated that currents lateral to apical dendrites are very small relative to currents occurring along the apical–proximal axis. The present paper outlines a two-dimensional method in which simultaneous samples are recorded from multiple electrodes in an equidistant array, enabling the continuous sensing of current flows in any direction within the plane of the slice, regardless of the relative orientation of the rows and columns of the array and the dendritic processes present in the slice. The array consists of 64 planar electrodes, each with a size of 50 × 50 μm, arranged in an 8 × 8 pattern with interpolar distances of 150 or 450 μm (Oka et al., 1999). After low-pass filtering at 100 Hz, the data were spatially smoothed by a 3 × 3-weighted average kernel (0 1/8 0, 1/8 1/2 1/8, and 0 1/8 0), and the result was convolved with a 3 × 3 Laplacian kernel (0 1 0, 1 −4 1, and 0 1 0) to produce a discrete approximation of the second spatial derivative. The medium was considered ohmic with a homogeneous conductance. The full correlation matrix was computed for all channels (64) in the time window considered (0–3 sec). Current-versus-time plots for single points in the slice were obtained by computing the 8 × 8 current source density for each time step and calculating the value at the desired location via bilinear interpolation. Well recognized limitations on the resolution affordable by current source density analysis arise from the relationship between the interelectrode distance (sampling resolution) and the radii of current sources or sinks occurring in the slice. The phenomenon of "aliasing," well known in the realm of computer graphics interfaces, refers to the occurrence of spurious data "ghosts" (aliases) when the distance between sampling points is larger than the size of the smallest phenomena to be represented. In computer screen graphics this occurs when the screen resolution is insufficient for the image being displayed (Fig. 1 *left*, *middle*). The appearance of spurious images on the screen is typically treated by "antialiasing" that incorporates low-pass filtering of the image with introduction of partially shaded pixels at the image's edges (Fig. 1, *right*). The present analysis uses low-pass filtering without full antialiasing; if the data contain phenomena with spatial frequencies too high to be resolved by the interelectrode sampling distances, the result is low-pass filtered to remove spurious aliases while also removing high-frequency data (Fig. 2).

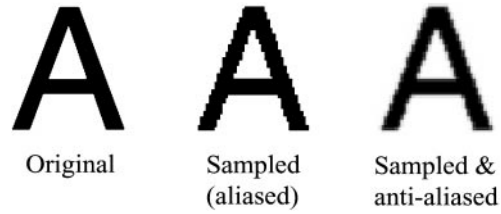

Figure 1. Aliases and antialiasing. *Left*, A high-resolution image with smooth edges is shown. *Middle*, The same image sampled with relatively low-resolution interpixel distance appears to have new features with high spatial frequency (the *jagged stair steps*). These "aliases" are introduced when the distance between adjacent sensors (pixels in this case) is insufficient to render the high-resolution image. *Right*, The same image sensed with the low-resolution pixels of the *middle panel* and antialiased is shown. Antialiasing includes a low-pass filter that removes the spurious alias features from the image and therefore may also (as in the present instance) eliminate some high-spatial frequency detail from the original image. The corresponding potential introduction of artifacts into array-sampled physiological data can be removed by the same antialiasing method (see Fig. 2 legend below) and will correspondingly eliminate some fine (high-spatial frequency) detail from the data.

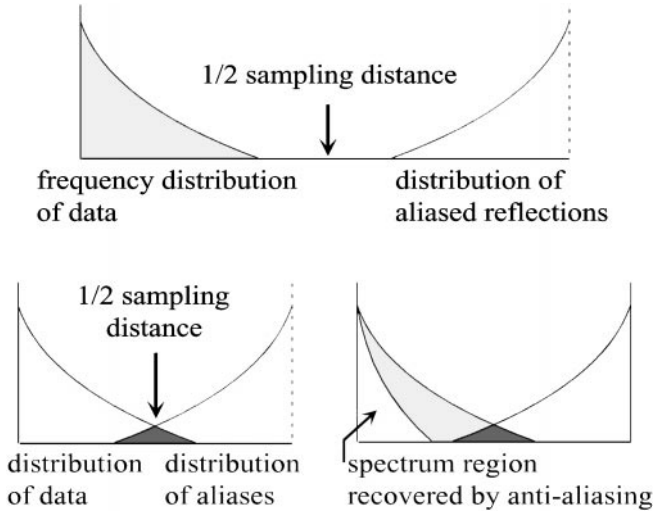

Figure 2. Effects of antialiasing. *Top*, An instance of intersensor spacing sufficient for the resolution of the sampled data is shown. Aliases appear as very high-frequency features; low-pass filtering at one-half the intersensor spatial frequency (double the intersensor distance) eliminates all aliases without reducing resolution of the sampled data. *Bottom*, Intersensor spacing insufficient for the resolution of the sampled data is shown. Spatial frequencies of aliases overlap the highest frequencies present in the data (*black region*). *Left*, Low-pass filtering at one-half the intersensor spatial frequency will fail to eliminate all the aliases and yet will eliminate some of the finest detail of the data. *Right*, Low-pass filtering at a lower spatial frequency successfully eliminates all spurious aliases and further reduces the resolution of the sampled data, eliminating much of the high-frequency fine detail that may be present in the measured data. Only lower frequency (larger) events remain.

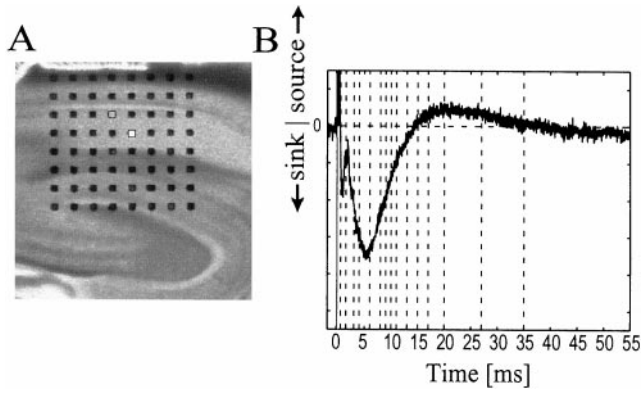

Figure 3. Measurement of evoked current. *A*, Placement of an 8 × 8 MED electrode *array*, with interelectrode spacing of 150 μm, centered in the apical dendritic field of CA1 in a hippocampal slice. The electrodes cover the basal dendrites of CA1, the apical dendrites of CA1, and the upper blade of the dentate gyrus granule cell field. *B*, EPSC elicited by a single pulse to the electrode marked in *white* in *A* and measured at the electrode in *gray* in *A*. To block GABA-mediated inhibitory components, 50 μM picrotoxin and 100 μM 2-hydroxysaclofen were applied. The time scale is typical for such evoked responses. *Vertical dashed lines* mark the time points for which measures will be taken across all 64 electrodes (see Fig. 4).

RESULTS

Continuous, two-dimensional current source density analysis

Two-dimensional current source density analyses were conducted in the context of stimulation of the Schaffer–commissural afferents to field CA1 in a hippocampal slice preparation. Figure 3 illustrates a typical experiment. To prevent the $GABA_A$- and $GABA_B$-mediated inhibitory components, this experiment was performed with 50 μM picrotoxin and 100 μM 2-hydroxysaclofen. Figure 3*A* shows the placement of the slice on the electrode array (interelectrode spacing, 150 μm). Figure 3*B* shows a typical postsynaptic current elicited by a single stimulation pulse to the electrode indicated in *white* and measured from the electrode in *gray*. The figure illustrates the time course and magnitude of the postsynaptic current at the indicated electrode, which is in the proximal portion of the apical dendrites of CA1. The direction of the current sink and source is as indicated; after the initial fiber volley (lasting ~1 msec) a current sink increases over a period of ~5 msec and decreases over the subsequent 5 msec before returning to baseline at ~13 msec. It becomes a current source and lasts for approximately another 15–20 msec before returning to baseline at ~35–40 msec. The relative magnitudes and time courses of the sink and source are typical for such evoked responses.

Two-dimensional current source density analysis was performed to obtain comparable measures of current sources and sinks of the same response. Figure 4 illustrates the continuous two-dimensional current source density analysis of the evoked response shown in Figure 3*B*. Each *panel* in Figure 4 illustrates the computed instantaneous sources and sinks in the slice, at selected times indicated by *vertical dashed lines* in Figure 3*B*. The array is positioned on the slice as shown in Figure 3*A*; the cell body layer of hippocampal field CA1 defines a *horizontal curve* approximately one-quarter of the way from the *top* of each *panel* in Figure 4. The *dashed lines* indicate the cell body layer of CA1 (*top*) and the boundary between stratum radiatum and stratum lacunosum/moleculare (*bottom*). Sinks are *blue* and sources are *yellow*, against a neutral background of *black*. It can be seen that after the initial fiber volley (lasting ~1 msec) a current sink in the apical dendrites of CA1 rises over a period of ~5 msec (see Figure 4, *6 msec panel*) and falls over the subsequent 5 msec before disappearing at approximately the *11 msec panel*. After an interim of ~2 msec during which currents are indistinguishable from neutral background, a source appears in the apical dendrites (Figure 4, *15 msec panel*) and lasts for approximately another 15–20 msec before disappearing at ~35 msec. The time courses and magnitudes of the waveform from a single electrode (Fig. 3*B*) can be seen to correspond closely to the computed current source density sink–source series in Figure 4.

Revealed by the two-dimensional current source density method are spatial aspects of the current sources and sinks that are difficult to discern by other means. The EPSC sink spreads across the apical field of CA1, in the region of Schaffer–commissural fibers presumably stimulated by the initiating current pulse (Fig. 4, *3–9 msec panels*); the ensuing current source occupies approximately the same zone (Fig. 4, *15–27 msec panels*). Both the sink and subsequent source occurring in the apical dendrites are accompanied by currents of reversed polarity in the basal dendritic field of CA1 (Fig. 4, near the *top* of each *panel*). Thus the predominant evoked response can be characterized as a current sink–source dipole that occurs from 3 to 9 msec and reverses to form a current source–sink dipole from 15 to 27 msec. Other, smaller currents are present in the slice but are not discussed here.

As described, the antialiasing performed in these analyses to prevent the introduction of artifacts attributable to aliasing will cause the loss of data with sufficiently high spatial frequencies. The filtering passes only those phenomena with spatial frequencies at most one-half that of the sampling frequency; in the present instance the interelectrode distance was 150 μm, preventing the measurement of current sources or sinks smaller than ~300 μm across (150 μm radius). This could be a redoubtable shortcoming in a structure the size of hippocampal field CA1, and it is expected that fine spatial detail will be lost in the method. It is instructive, therefore, to examine the spatial resolution of the CSDs measured by this method. Figure 5 depicts the boundaries of the apical dendrites of field CA1 superimposed on the region of measurement. Figure 5, *left*, shows the slice and the position of the array (from Fig. 3); Figure 5, *right*, is the instantaneous CSD in the region of the electrode array (from Fig. 4), at 6 msec after stimulation at the indicated electrode. The *dashed lines* (Fig. 5, *right*) indicate the cell body layer of CA1 (*top*) and the boundary between stratum radiatum and stratum lacunosum/moleculare (*bottom*). The primary measured current sink (*blue*) occupies only the region where apical dendrites occur, and the reciprocal current source (*yellow*; *top*) occurs only in the region of basal dendrites. (An absence of current appears in the computed image at the location corresponding to the stimulating electrode; no recordings were taken from that electrode, and the resulting CSD processing leaves a gap.) It can be seen that the borders of the computed sink do not coincide precisely with the location of the anatomical limits of the dendritic field, inaccuracies that may result from the resolution limits of the method.

Distribution and current sources for carbachol-induced β waves within the hippocampus

Figure 6*A* contains a micrograph of a hippocampal slice and underlying 64-electrode array with 450 μm between recording positions (the "broad array"). Baseline activity was of low voltage and generally devoid of synchronous activity, and there were no reliable differences between subfields (Fig. 6*C*). Infusion of carbachol was followed by a gradually developing rhythmic activity in the pyramidal cell fields that was close to or within the β band (10–30 Hz) in 41 of 55 slices tested (Fig. 6*D* for an example). Thirty-four of those 41 slices had β band oscillations in both CA1 and CA3. Low-voltage activity at the upper end of the θ range was observed in either field CA1 or CA3 in the remaining seven cases. The relative prominence in CA1 versus CA3 was not consistent across slices. Synchronous high-frequency activity was also found in the dentate gyrus, much more so in the internal than in the external wing of the structure (Fig. 6*B,D*). Throughout the pyramidal cell fields, the waves were larger in the apical than in the basal dendrites and typically had phase reversals between the two loci, as can be seen in the higher gain record shown in Figure 6*E*.

Fast Fourier transforms were used for quantitative analysis of the frequency and distribution of the carbachol-induced rhythms. For the example illustrated in Figure 6*B*, most of the power in the

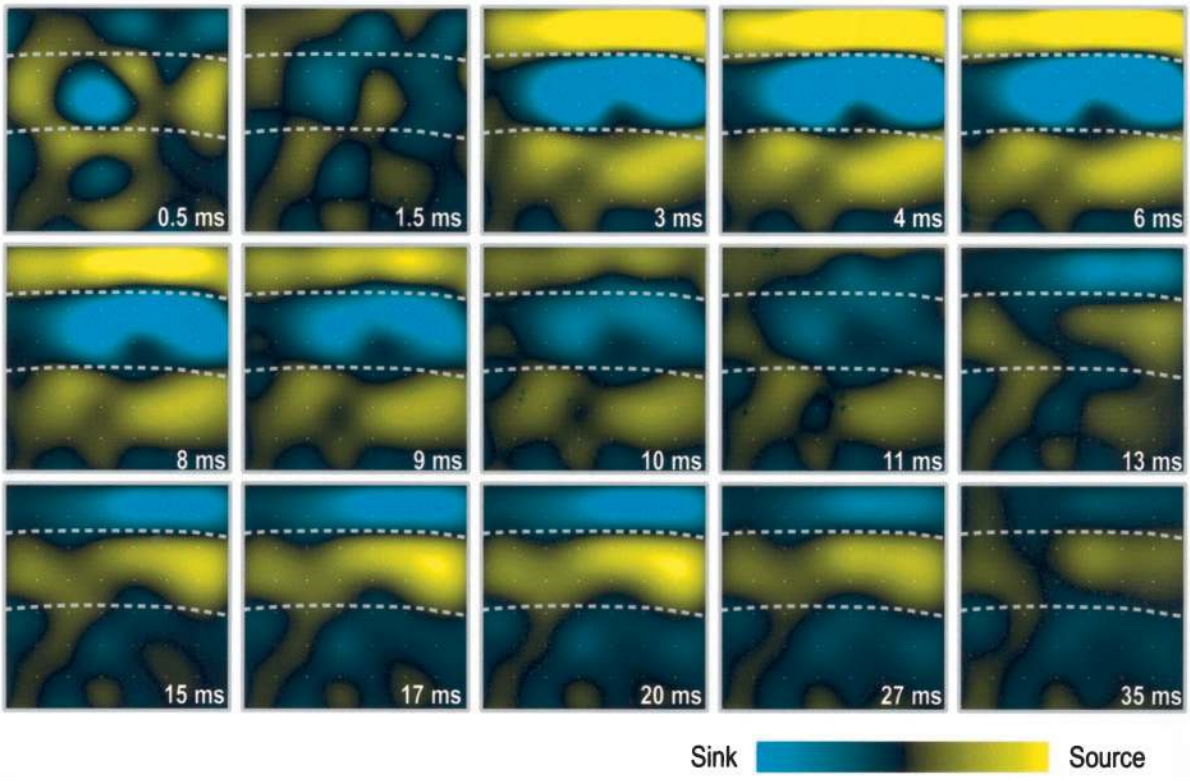

Figure 4. Continuous two-dimensional current source density analysis of evoked response. Shown are the computed instantaneous two-dimensional current source density plots across all electrodes at each of the time points indicated in Figure 3*B* by *vertical dashed lines*. At the *bottom right* of each *panel* are the times in milliseconds after the application of a pulse to the *white* electrode of Figure 3*A*. As shown in the *horizontal bar* at the *bottom right*, sinks are *blue* and sources are *yellow* against a current-neutral background of *black*. The limits of the stratum radiatum in CA1 are indicated by *horizontal dashed lines*. The stimulating electrode cannot be recorded from, resulting in a singularity that is visible in the sink field in approximately the *top middle* of each *frame*. After an initial response because of the fiber volley, a current sink spreads rapidly through the dendritic zone of field CA1 (with the singularity appearing at the site of stimulation). The sink intensifies and expands over ~5 msec and then fades, disappearing at ~10 msec. After a brief pause, a current source appears in these dendrites, with its center slightly more distal than that of the current sink. The apical source intensifies, expands, dissipates, and disappears by ~35 msec, making the "period" of the evoked response ~35 msec. Both the apical sink and ensuing apical source are accompanied by a field of reversed polarity appearing in the basal dendrites of CA1 (*top* of each *panel*) that grows and dissipates with approximately the same time course as the apical events.

spectrum was found between 10 and 30 Hz with a definite peak at 20 Hz. The group mean for the dominant CA1 frequency for all slices was 18.8 ± 5.7 Hz (mean ± SD) and 19.2 ± 4.8 Hz for the β instances alone. The equivalent values for CA3 were 16.4 ± 5.7 and 17.3 ± 4.2 Hz. The differences between CA3 and CA1 did not reach statistical significance. The recording sites with the greatest power in the 10–30 Hz band were located in the apical dendrites of field CA3 and CA1, typically in the more distal fields.

Arrays with 150 μm spacing (the "dense array"; Fig. 7*A*) provided finer spatial resolution of the rhythmic activity. Recording centered on the CA3–CA1 border revealed a surprisingly steep gradient of absolute potentials in the distal-to-proximal dimension with the largest potentials occupying a discrete region corresponding to the stratum moleculare of fields CA3a and b (Fig. 7*B*). It is noteworthy that potentials reversed across the cell layer boundary (see, e.g., Fig. 7*B*, *top left quadrant*). Lesser although still substantial voltage bands are also present in CA1. The frequency spectra for all channels are shown in Figure 7*C*. All the observed oscillatory activity was absent in the presence of blockers of either glutamate or GABA.

Continuous two-dimensional current source density analyses were conducted to define further the sources of these cholinergically induced oscillations. Figure 8 illustrates the instantaneous sources (*yellow*) and sinks (*blue*; against a neutral background of *black*), at 4 msec intervals from an arbitrarily chosen starting time of 0, in the same slice and during the same spontaneous activity shown in Figure 7. The *outlines* of the granule and pyramidal cell fields and the extents of their apical dendrites have been superimposed to illustrate the locations of events occurring during the time

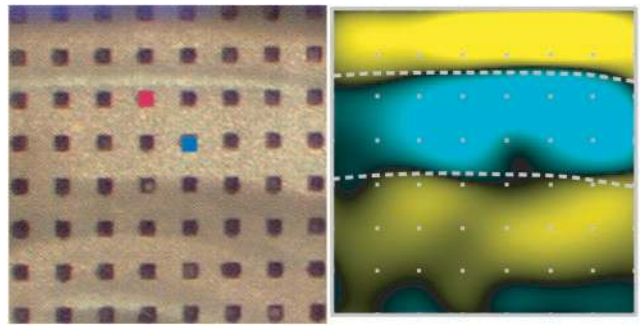

Figure 5. Alignment of computed physiological phenomena with known anatomical structure. *Left*, Placement of the electrode *array* on the hippocampal slice (close-up of Fig. 3*A*). The *top* of the *array* coincides with the basal dendrites of CA1, the *top-middle portion* of the *array* overlays the field of apical dendrites in CA1, and the *bottom third* of the *array* overlays the upper blade of the dentate gyrus. *Right*, The physiological response computed by continuous two-dimensional current source density analysis 6 msec after the stimulation of a single electrode (indicated in *blue*). The *image* is a close-up of the 6 msec *frame* from Figure 4. The limits of the stratum radiatum in CA1 are indicated by *dashed lines*. It can be seen that the extent of the evoked current sink closely corresponds to the limits of the apical dendrites. An apparent hole in the current sink occurs at the site of the stimulating electrode, where no recording is performed and no current source density is computed. There is little current in the cell body layer itself, and current source appears in the basal dendrites (*top* of *panel*). There is little current at the apical tips of the CA1 dendrites (*middle* of *panel*) and some less intense current sources occurring in the stratum lacunosum/moleculare.

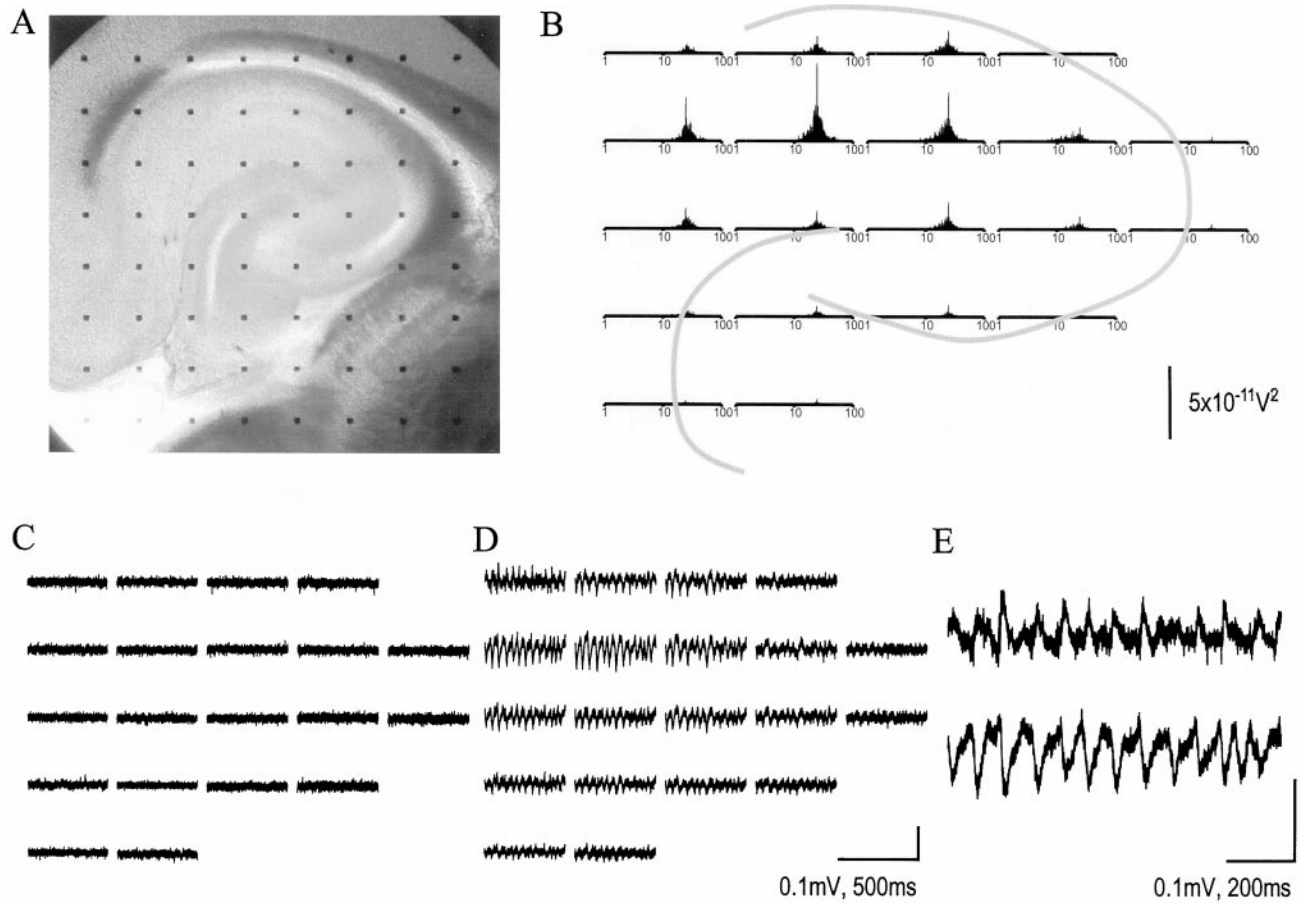

Figure 6. Distribution of carbachol-induced β waves within the hippocampus. *A*, Micrograph of hippocampal slice on the MED probe. Subfields of the hippocampus and overlying cortex can be seen, and the broad *array* of electrodes, with an interelectrode spacing of 450 μm (see Materials and Methods), is shown. *B*, Spectra of carbachol-induced spontaneous activity at 20 electrode sites that contact part of the hippocampus in the slice. Each *x*-axis is on a logarithmic scale from 1 to 100 Hz. Activity is seen in the 10–30 Hz frequency range, especially in apical dendrites of fields CA1 and CA3, with lower levels of activity elsewhere. *Gray lines* indicate the position of the pyramidal and granule cell fields. *C*, Samples of activity at the same 20 electrodes in baseline conditions. *D*, Activity measured after infusion of 50 μM carbachol. *E*, Close-up of carbachol-induced activity in the *top left* electrodes in the *array*, indicating the reversal of polarity across the cell body layer of field CA1. Calibration bars: *B*, 5×10^{-11} V^2; *C, D*, 0.1 mV, 500 msec; *E*, 0.1 mV, 200 msec.

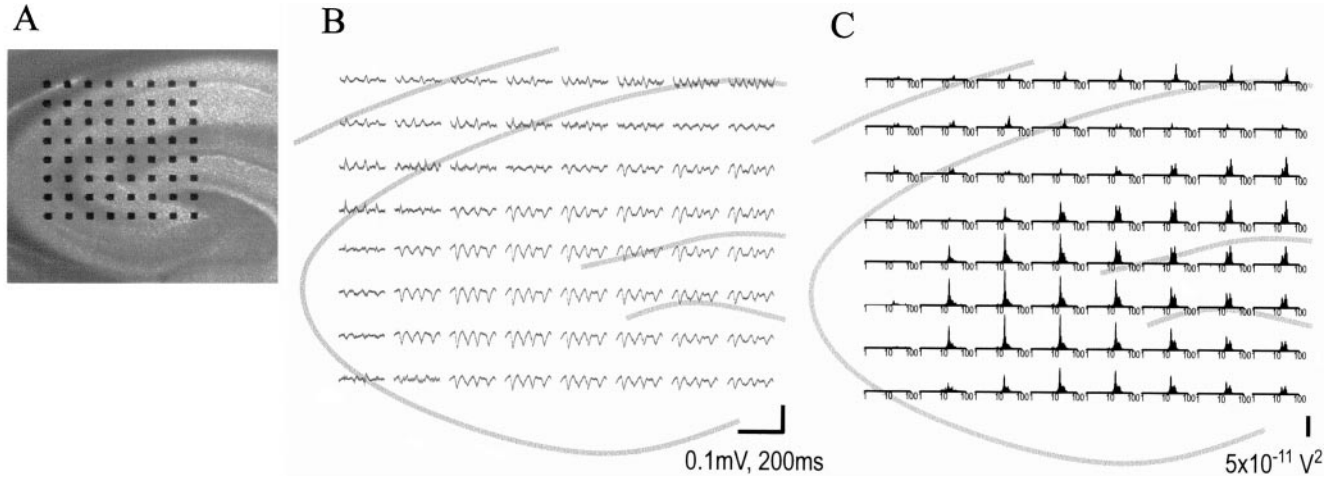

Figure 7. Carbachol-induced β waves in the hippocampus measured with a dense electrode. *A*, Micrograph of a hippocampal slice on a dense-array probe, with electrodes spaced 150 μm apart. *B*, Sample of spontaneous responses in the presence of 50 μM carbachol. A sharp gradient between rhythmic versus low-intensity activity is evident along the proximoapical axis in both CA3 and CA1. The polarity of the responses is reversed across the cell body layer boundary, as is visible in the *top left quadrant* of the *panel*. *C*, Power spectra of carbachol-induced spontaneous responses, with the same log *x*-axis as in Figure 6*B*. The gradient between rhythmic and less rhythmic activity can be seen. Calibration bars: *B*, 0.1 mV, 200 msec; *C*, 5×10^{-11} V^2.

period. A large sink in apical CA1 is accompanied by a source in the basal dendrites of CA1. The sink and its accompanying basal source intensify and expand over the course of ~12 msec, and both subside to approximate baseline levels by ~16 msec after initial appearance. After a brief period characterized by currents that are barely distinguishable from background, a source arises in apical CA1, accompanied by a sink in the basal dendrites of CA1. The source (and its accompanying dipole) lasts for ~20 msec before

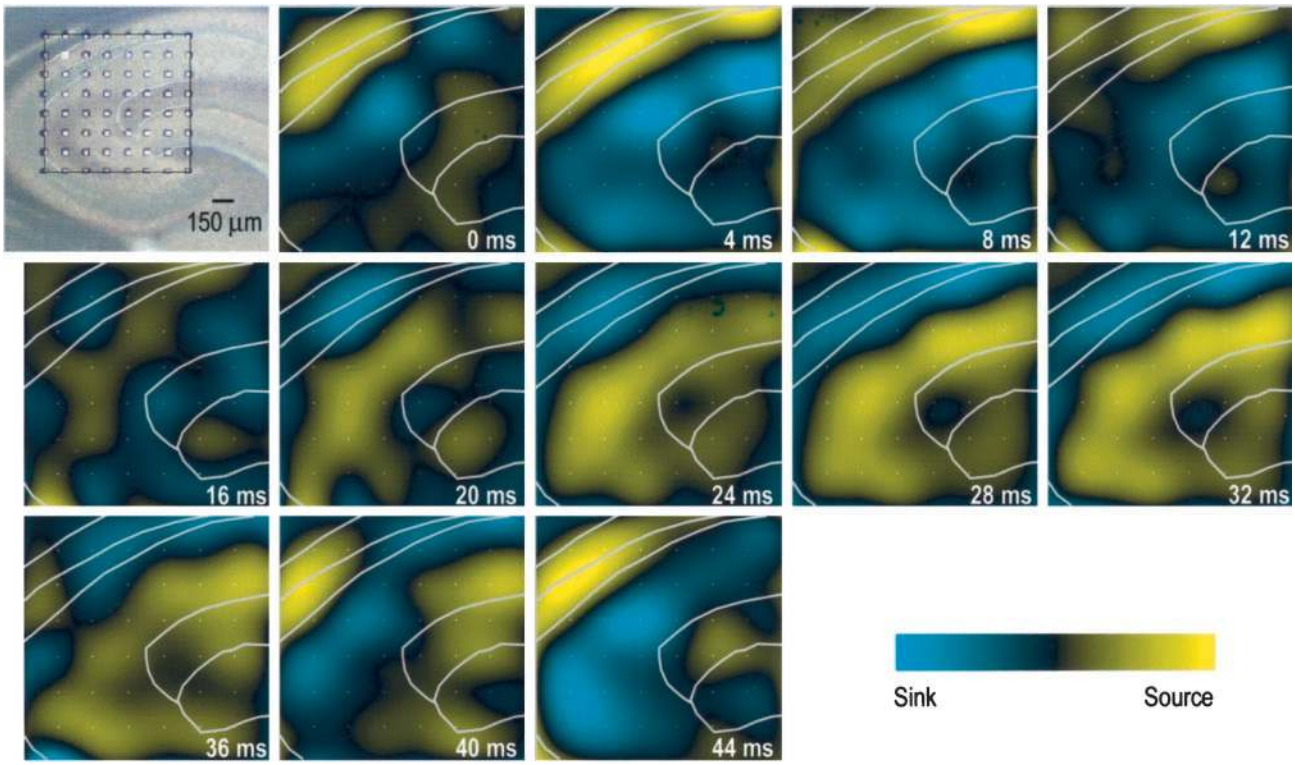

Figure 8. Current source density analyses of carbachol-induced activity. In the same slice as in Figure 7, the *outlines* of the pyramidal and granule cell fields and their apical dendrites are shown. The *array* includes parts of the pyramidal cell fields of CA3 and CA1 and their apical dendrites and part of the upper blade of the dentate gyrus. Each *frame* shows the instantaneous computed current source density in the region of the electrode *array*. From an arbitrarily chosen starting point, a sink appears in the apical dendrites of the border between fields CA3 and CA1, with an associated source across the cell boundary layer in the basal dendrites. Within a few milliseconds, an additional focal sink has appeared in apical CA1 with a corresponding basal source. The fields merge and intensify and then dissipate after ~12 msec. After a brief interim during which activity is not distinguished from background, a source appears in the apical dendrites at ~20 msec, with a corresponding sink in the basal dendrites. These expand and intensify before dissipating by ~20 msec later (40 msec), after which an apical sink reappears to reinitiate the cycle. The cycle repeats indefinitely (as indicated in the next figure), with an approximate frequency of 25 Hz.

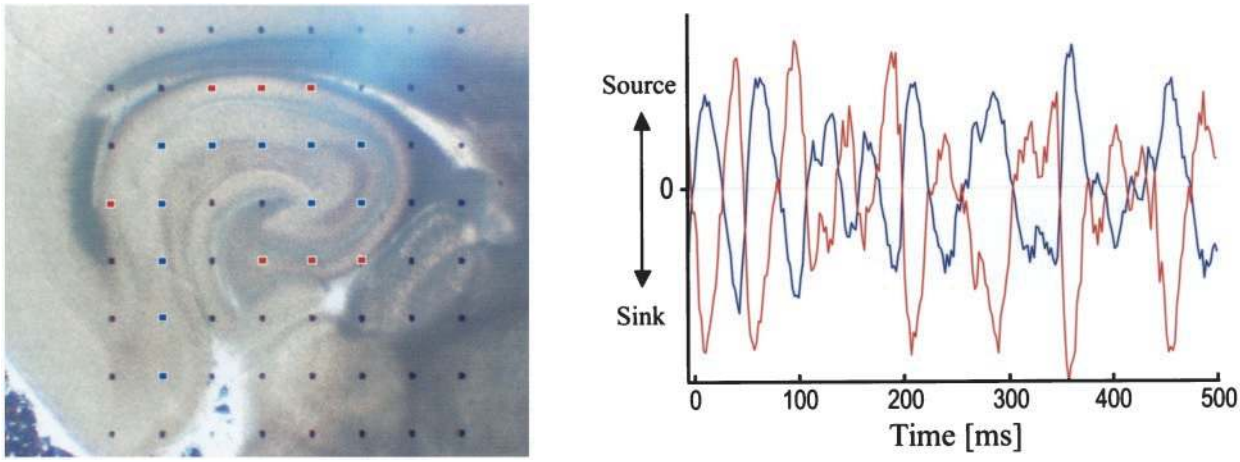

Figure 9. Relationship of recurring carbachol-induced oscillations in apical and basal dendrites. *Left*, Hippocampal slice on a broad (450 μm interelectrode spacing) *array*. The electrodes used to measure basal dendritic responses of pyramidal cell fields are indicated in *red*; those used to measure apical dendritic responses are in *blue*. *Right*, Averaged responses from apical (*blue*) and basal (*red*) dendritic fields shown over 500 msec (0.5 sec) of elapsed time. Carbachol-induced (20 μM) oscillations were sustained across all sampled periods, as in this typical response. Average apical and basal responses are reversed in polarity, i.e., are 180° out-of-phase. The frequency of the waves is 23.1 ± 0.8 Hz (mean ± SE).

dissipating. It is noteworthy that the apical source appears to have its center more distally located than that of the more focal apical sink preceding it, to within the resolving power of the interelectrode spacing of 150 μm. The sink–source dipole recurred and gave rise to the frequency plot shown in Figure 7; the time course from peak to peak of this recurring apical sink–source dipole was ~40 msec, consistent with a frequency of ~25 Hz. The source–sink and sink–source dipoles and their sharply defined boundaries between sources and sinks along the pyramidal cell body layer were recurring features across many experiments, as was the latency from one apical sink through an apical source to the next apical sink, as seen in Figure 9, which shows a typical record of the repetitive oscillations induced by carbachol in a slice. Shown are the averaged sinks and sources occurring in the apical dendrites, as measured from the electrodes marked in *blue*, and in the basal dendrites (*red* electrodes). The apical versus basal oscillations retain a relationship of

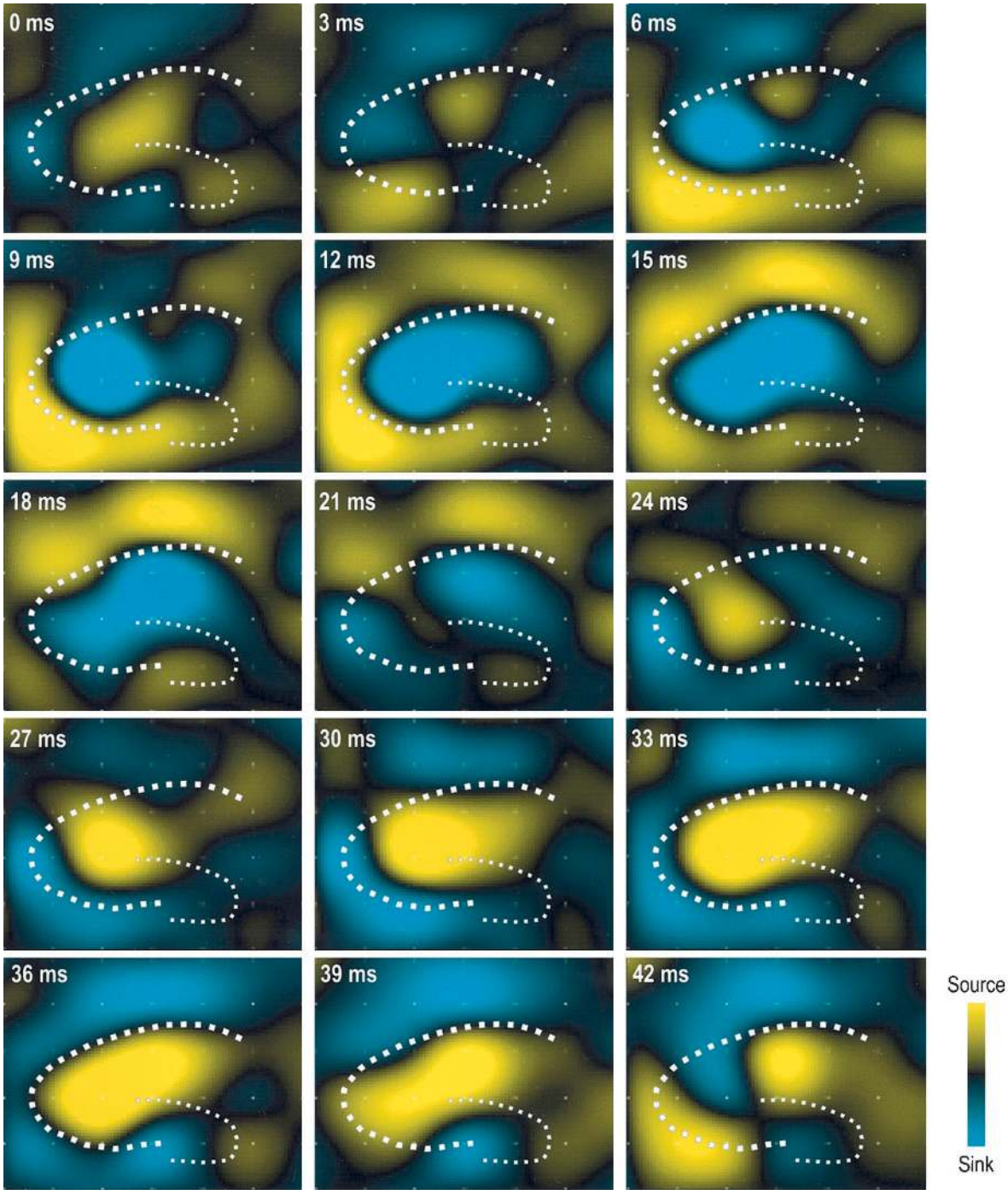

Figure 10. Evolution of current source density over time (42 msec). Each *frame* shows the computed current source density at a particular millisecond (indicated at the *top left* of the *frame*) during the recording of spontaneous activity with a broad (450 μm spacing) *array*. *Blue* indicates the maximum magnitude of sinks; *yellow* indicates the maximum magnitude of sources. The positions of the pyramidal and granule cell fields are indicated by *dashed lines.* Beginning at arbitrarily chosen time 0, an intense focal sink in the apical dendrites of field CA3 begins at ~6 msec, accompanied by sources in the cell and basal dendrite layers of CA3. The sink continues through ~12 msec before beginning to expand toward field CA1. The sink in apical CA3 dissipates at ~18 msec, followed ~3 msec later by the apical sink in CA1. The basal sources dissipate at approximately the same time as their associated apical sinks. An apical source begins in CA3 at ~24 msec, accompanied within a few milliseconds by a mild basal source in CA3; the apical source then expands toward CA1, with an accompanying basal sink in CA1. These source–sink pairs then dissipate after ~15–20 msec. Such cycles recur irregularly in this slice. (This series of *frames* and other related series can be viewed at http://www.med64.com/publications.htm.)

opposite polarity throughout the measured period, and the frequency of the observed oscillations remains relatively stable at 23.1 ± 0.8 Hz across multiple 1 sec samples. The sustained occurrence of alternating current source–sink dipoles across the cell body layers of CA3 and CA1, within the range of 10–30 Hz (β), is robustly observed in the majority of slices and time periods sampled.

Shifts between sinks and sources over larger areas were assessed with continuous two-dimensional current source density analyses using an electrode array with interelectrode spacing of 450 μm, as opposed to all previous current source density examples that used arrays of 150 μm distances. The resulting aliases and antialiasing (see Fig. 2) necessarily entail further loss of resolution; for an interelectrode spacing of 450 μm and concomitant antialiasing, the smallest events that can reliably be imaged are those with a radius of 450 μm (diameter of 900 μm) or larger. Figure 10 shows a typical

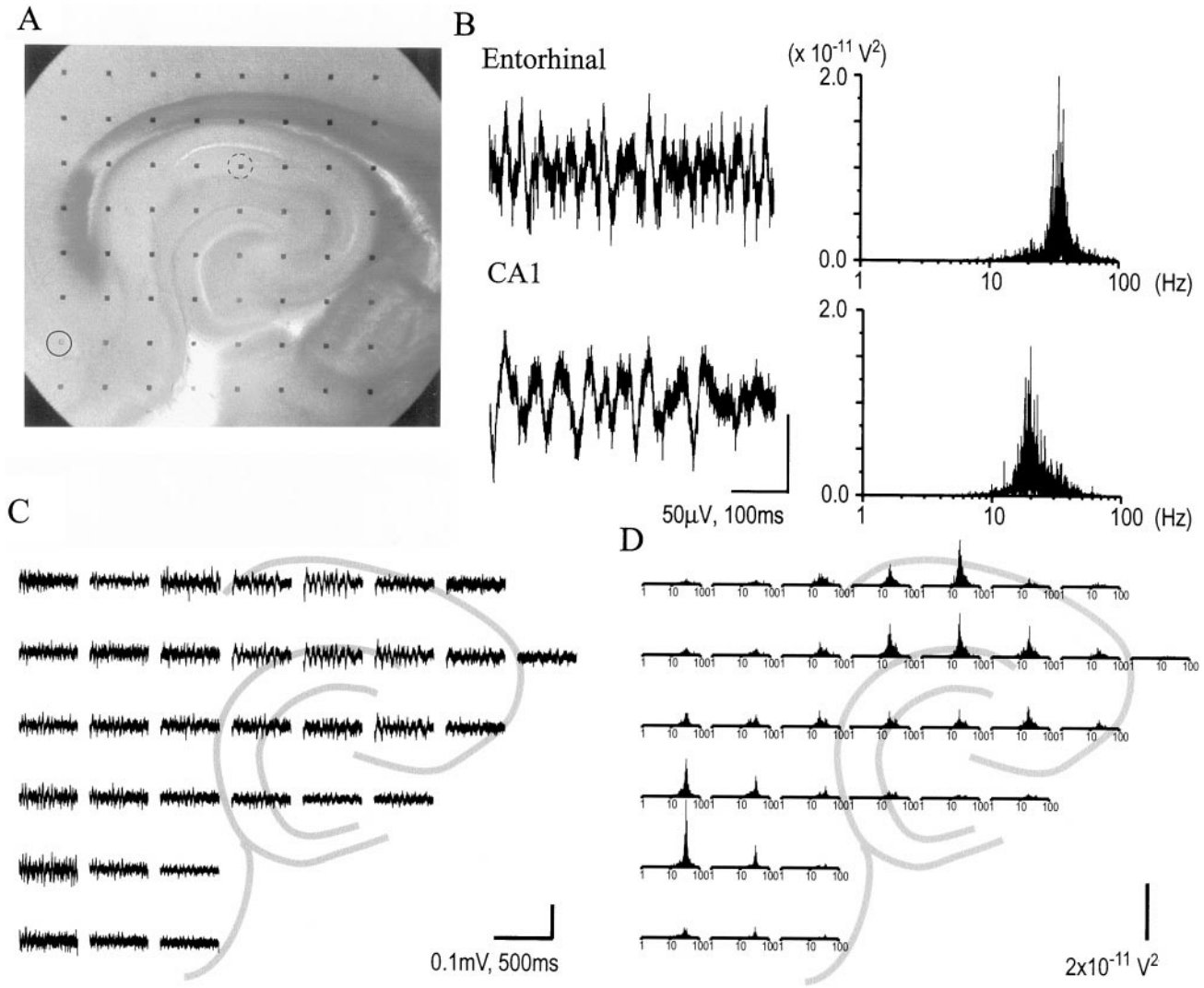

Figure 11. Two distinct carbachol-induced rhythms in the hippocampus and cortex. *A*, Micrograph of a corticohippocampal slice on a broad *array*. Two sites are indicated in the apical dendrites of field CA1 (*dashed circle*) and the deep layers of entorhinal cortex (*solid circle*). *B*, Sample activity in response to the infusion of carbachol (50 μM) from the selected electrodes in entorhinal cortex and field CA1 (*left*) and power spectra for recordings over 3 sec at these two sites (*right*). Power values are given as $\times 10^{-11}$. Although field CA1 exhibits β-like rhythm centered at ~20 Hz, carbachol elicits higher frequency (35–40 Hz) activity in entorhinal cortex (*top right spectrum*). *C*, Distribution of representative activity in the slice. *D*, Distribution of low-pass (0–100 Hz) filtered power spectra in the slice. *Gray lines* indicate the position of the pyramidal and granule cell fields. Calibration bars: *B, left*, 50 μV, 100 msec; *C*, 0.1 mV, 500 msec; *D*, 2×10^{-11} V^2.

cycle. At arbitrarily chosen time 0 msec, a weak current source in the apical dendrites of field CA3 is surrounded by diffuse sources centered on the pyramidal cell layers. Six milliseconds later a discrete but intense sink develops in the proximal st. radiatum of CA3 that is accompanied by sources in the basal dendrites of CA3. The sink grows, and a fully developed sink–source relationship centered on CA3b is in evidence at the 9 msec time point (Fig. 10). The sink then extends into the st. radiatum of CA1 accompanied by the appearance of a pronounced cell body/basal dendrite source at 15 msec. Note that by this time point the sink–source relationship in CA3 has begun to collapse. By 24 msec a pronounced current source has developed in the distal dendrites of field CA3 that grows in intensity and begins to extend into the distal dendrites of field CA1 (see Fig. 10, 30 msec time point). This source is reasonably stable and occupies much of the distal apical dendrites for the following 10 msec (see Fig. 10, 39 msec time point) and returns to the starting pattern at 42–45 msec. In all then, the wave involves an intense apical dendritic sink lasting ~10 msec followed by an apical source lasting for approximately twice that period. These events begin in CA3 and are seen in CA1 within 3–5 msec. Data of a similar type from the entorhinal–hippocampal system suggest that propagation of activity involves interactions between reverberating circuits (Iijima et al., 1996). Repetitive stimulation provided by reverberating circuits may drive the spread of activity from one region to another.

These observations show that relatively brief apical sinks are interposed between the longer lasting apical sources. Examination of averaged currents demonstrated that distribution of sources and sinks across the pyramidal cell subdivisions of the hippocampus varied between slices. Between-slice variability was also present in serial current source density analysis with major differences in the degree to which events were centered in CA3 versus CA1. However, the brief apical sink–longer apical source sequence for the apical dendrites was prominent in all slices exhibiting oscillations in the β range.

Carbachol induces a 40 Hz rhythm in retrohippocampal cortex

The question of whether the rhythms elicited by carbachol are regionally differentiated was addressed by close examination of those slices in which the electrode array was positioned underneath a significant portion of the retrohippocampal cortex field along with the pyramidal cell fields of the hippocampus itself. Figure 11*A* shows a case in which the broad array (450 μm spacing) had a row

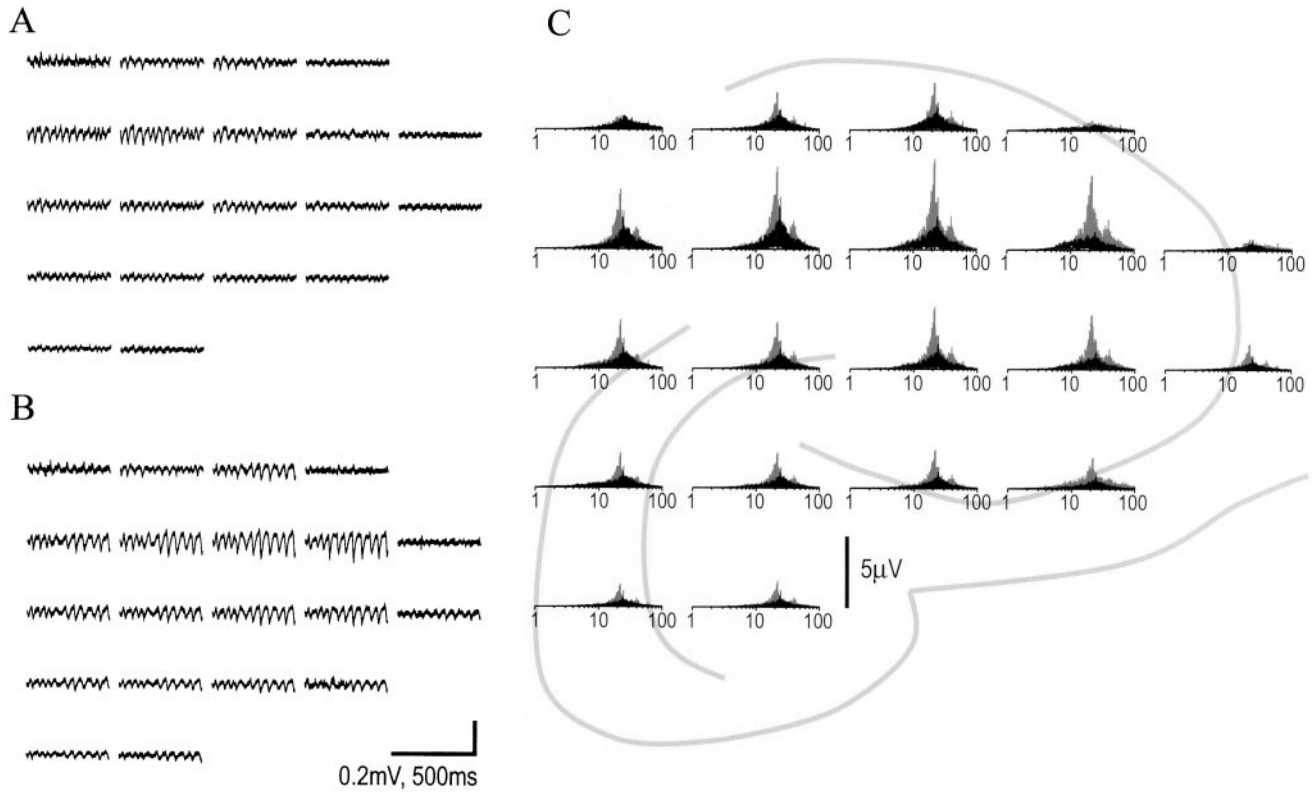

Figure 12. Effect of benzodiazepines on carbachol-induced β waves. *A*, β Rhythm activity induced by 20 μM carbachol. Largest responses arise in apical dendrites of fields CA1 and CA3. *B*, Activity in the same slice after infusion of 3 μM diazepam. Rhythmic activity is greatly enhanced and spreads to regions that were relatively inactive. *C*, Superposition of power spectra in the absence (*black*) and presence (*gray*) of diazepam. Power in the β frequency is enhanced by as much as threefold, without much shift in the frequency. In addition, a peak is added at a higher (~40 Hz γ) frequency by the addition of diazepam. *Gray lines* indicate the position of the pyramidal and granule cell fields. Calibration bars: *A, B*, 0.2 mV, 500 msec; *C*, 5 μV.

underneath the deep layer of the entorhinal cortex. Carbachol-induced fast waves from the indicated positions in field CA1 and entorhinal cortex are compared in Figure 11*B*. As can be seen, the entorhinal oscillations have a higher frequency than do those from the hippocampus. Fast Fourier transforms indicate that the dominant frequency in the cortex is approximately twice that in field CA1. Results for all recording sites are summarized in Figure 11*C*. Rhythmic activity with a peak near 20 Hz is found via the apical dendrites of the hippocampal pyramidal cell fields, whereas 40 Hz activity is predominant at the entorhinal sites. It can also be seen that the 40 Hz oscillations are centered in the deep layers of the medial entorhinal cortex. Regions lying between the hippocampus and medial entorhinal cortex have both peaks. Indeed, it appears that the relative balance of 40 versus 20 Hz increases in an orderly manner across the series of steps included in the retrohippocampal cortex. Forty Hertz activity was recorded in the deep layers of the entorhinal cortex in each of the 15 slices that had appropriately positioned electrodes; it thus appears to be a characteristic response of this region to cholinergic stimulation. This is not unexpected considering that carbachol was reported to induce 40 Hz oscillations in the medial entorhinal cortex of isolated guinea pig brain (van der Linden et al., 1999).

Transmitter systems involved in carbachol-induced β waves

Carbachol-induced high-frequency rhythms were completely eliminated by 20 μM atropine and greatly reduced by the AMPA receptor antagonist CNQX (20 μM). In the presence of bicuculline (10 μM), muscarinic stimulation produced high-frequency spiking in the stratum pyramidale and in some instances epileptiform discharges, but rhythmic activity was absent. Under these conditions, carbachol initiated repetitive bursting behavior and occasional seizures. The interval between the epileptiform bursts sometimes approximated the period of the θ wave (data not shown). The observed seizure activity resembles that reported by Williams and Kauer (1997).

Table 1. Summary of eight experiments in which carbachol-induced high-frequency rhythms were present in a hippocampal slice before infusion of diazepam

Slice number	CA3 (%)	CA1 (%)
1	639	521
2	344	264
3	414	211
4	197	119
5	431	200
6	177	213
7	132	117
8	235	90
Mean ± SD	321 ± 170	217 ± 137

Shown are the maximal percent increases in power at the peak frequency in fields CA3 and CA1.

Benzodiazepines markedly enhanced the amplitude of β oscillations as can be seen in Figure 12, compare *A* (carbachol alone) and *B* (carbachol plus 3 μM diazepam). A Fourier transform indicates that the increased amplitude is not accompanied by a significant change in the frequency of the waves. Figure 12*C* summarizes the frequency spectra for recording loci within the hippocampus. This shows that diazepam (Fig. 12*C*, *gray spectra*) not only caused a nearly threefold increase in power within the 20 Hz band over carbachol alone (Fig. 12*C*, *black spectra*) but also gave rise to a second carbachol-triggered peak at ~40 Hz. Table 1 summarizes the results for eight experiments in which carbachol-induced high-frequency rhythms were present before the infusion of diazepam.

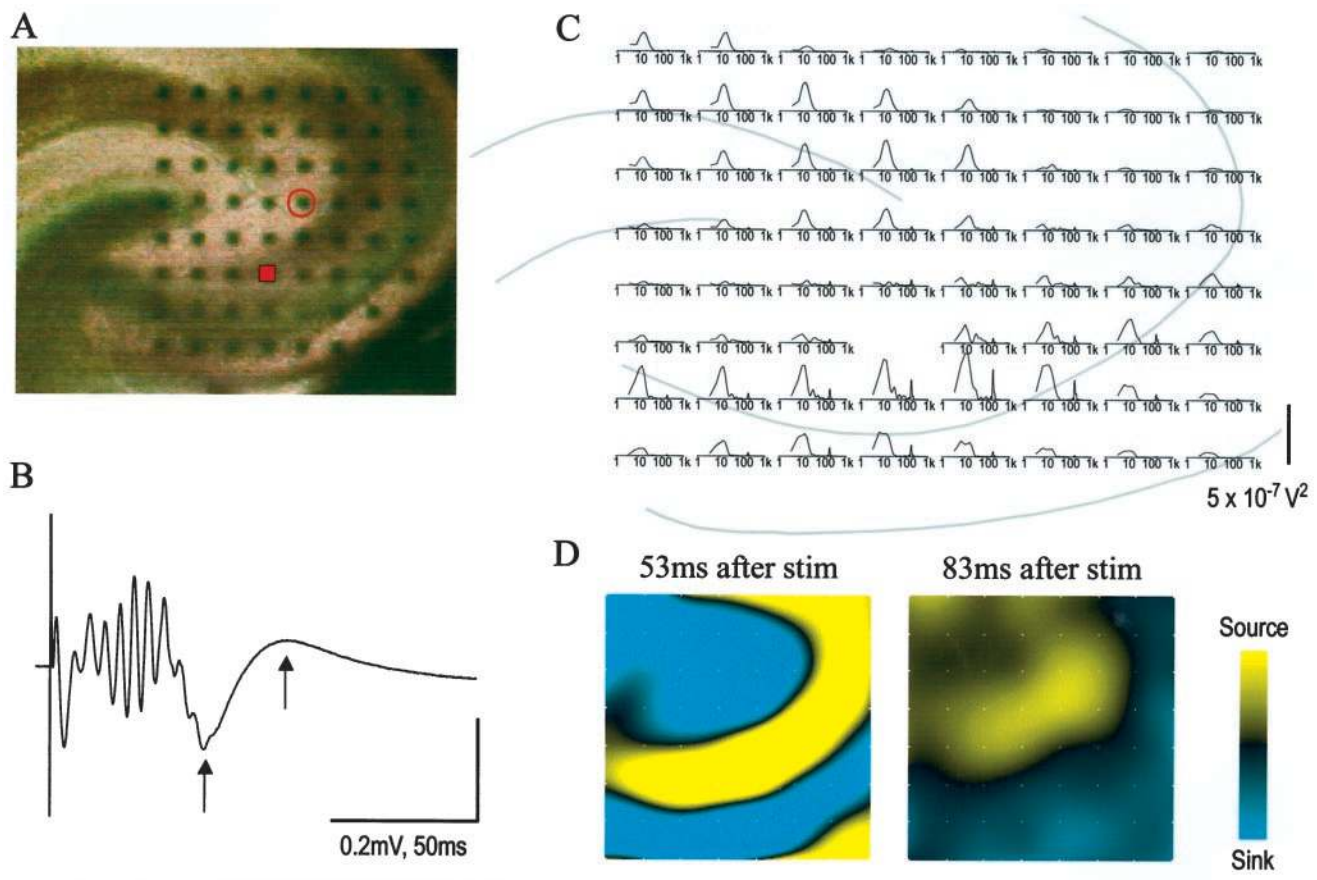

Figure 13. Two-dimensional current source density analysis of β-like activity elicited by orthodromic activation of field CA3. *A*, Position of the *array* (150 μm interelectrode spacing) on a hippocampal slice, centered in field CA3. *B*, Typical response to orthodromic stimulation of field CA3. Stimulation was induced at the electrode indicated by a *solid color* and was recorded at the *circled* electrode in *A*. The response exhibits a small burst of spikes followed by a positive-going wave lasting ~30–40 msec. *Arrows* indicate the peak sink (53 msec) and peak source (83 msec). *C*, Distribution of power spectra in the slice. The largest responses are in apical dendrites of CA1 and apical and proximal dendrites of CA3. Frequency peaks occurred at 15–20 Hz and at 100–200 Hz; note that the log scale used extends from 1 to 1000. *D*, Two-dimensional instantaneous current source density analyses at two time points (53 and 83 msec after stimulation, indicated in *B* by *arrows*). At 53 msec, the evoked current sink is at its peak and can be seen to occur predominantly in the apical dendrites of CA3, with a corresponding source in the basal dendrites. At 83 msec, the rebound source peaks; it can be seen also to occur in the apical dendrites of CA3, with a corresponding sink in the basal dendrites. *stim*, Stimulation. Calibration bars: *B*, 0.2 mV, 50 msec; *C*, 5×10^{-7} V^2.

The increase in power at peak frequency was 321 ± 170% for CA3 and 217 ± 137% for CA1. Within-slice effects of diazepam were correlated ($r = 0.93$), and the increase in CA3 was statistically greater than that in CA1 ($p < 0.05$, paired t test, two tails). The frequency of the oscillations after diazepam was correlated across slices with that recorded under carbachol alone (CA3, $r = 0.85$; CA1, $r = 0.96$).

Orthodromic activation of pyramidal cells triggers β-like activity in the apical dendrites

How the GABAergic cells responsible for apical sources are activated is clearly of importance for understanding the origins of β oscillations. If pyramidal cell collaterals are involved, then orthodromic stimulation sufficient to cause repetitive spiking should result in the appearance of β-like activity in the areas in which the carbachol-elicited rhythms are found. Single-pulse stimulation of the Schaffer–commissural fibers does not typically cause repetitive spiking because (1) the potent feedforward dendritic inhibition in the stratum radiatum shunts the excitatory current and (2) perisomatic inhibition prevents repetitive discharges. Concentrations of bicuculline that partially block the GABAa receptor pool were used to reduce these inhibitory responses and thereby allow the pyramidal cells to emit four to five spikes in response to orthodromic stimulation. Figure 13*B* shows a typical response that is composed of a string of population spikes followed by a positive-going wave. Fourier transforms showed that the frequency spectrum for the response had peaks at 15–20 and 100–200 Hz (Fig. 13*C*). As can be seen, the 15–20 Hz component was pronounced in the distal apical dendrites and had a distribution similar to that of carbachol-induced β waves. Responses of the type described in Figure 13 were sensitive to bicuculline concentrations and were blocked by it at 20 μM. Current source density analyses of the late evoked response showed a source that ran in the stratum radiatum ~200–400 μm above the st. pyramidale from the stimulation site near the hilus toward CA1; this was paralleled by a dense sink in the cell bodies and basal dendrites (Fig. 13*D*).

DISCUSSION

Simultaneous recording from a large number of sites revealed that cholinergic stimulation triggers β range oscillations within both pyramidal cell subfields of the hippocampus. The rhythms were phase shifted across the pyramidal cell layers indicating that they were locally generated by sinks and sources aligned along the long axis of the pyramidal cells. Current source density analyses confirmed that carbachol generated negatively correlated apical and basal currents. These analyses also showed that the apical dendrites were on the average a source for more proximally located sinks. The simplest explanations for these relationships are that carbachol-induced oscillations reflect (1) depolarizing currents in the basal dendrites and regions proximal to the cell bodies or (2) hyperpolarizing currents in the apical dendrites. Examination of how current source densities varied across the period of an individual β wave showed that 10-msec-long current sinks in the prox-

imal apical dendrites were followed (or preceded) by apical current sources lasting for ~20 msec. This is highly suggestive of an arrangement in which EPSPs alternate with the more persistent IPSPs. Because the former are associated with depolarization and spiking of pyramidal cells, then β activity could arise from an oscillatory circuit in which tonically excited pyramidal cells activate interneurons that produce dendritic IPSPs that suppress further pyramidal cell firing. Dissipation of the IPSPs would then be followed by pyramidal cell discharges and a new cycle. As discussed below, this argument regarding the origins of β rhythms accords with known effects of cholinergic stimulation on hippocampal cells.

It is well established that carbachol blocks IPSPs, most probably by suppressing release (Behrends and Bruggencate, 1993). It also increases the excitability of inhibitory interneurons, as evidenced by the increased frequency of spontaneous IPSPs (Pitler and Alger, 1992; Behrends and Bruggencate, 1993). These results point to the conclusion that cholinergic stimulation facilitates some interneurons and suppresses others. In accord with this, anatomical studies have localized M-2 receptors to basket cell terminals in the stratum pyramidale and to the dendrites of a distinctly different population of GABAergic neurons in the stratum oriens/stratum radiatum (Levey et al., 1995; Hajos et al., 1998). Double-labeling experiments established that these latter neurons form dense terminal fields in the distal apical dendrites of pyramidal neurons (Hajos et al., 1998). It can therefore be expected that the two populations of muscarinic receptors just noted will have the effect of suppressing GABA release from basket terminals while increasing the excitability of a discrete subgroup of interneurons that generate IPSPs in distal apical dendrites. This latter event is an obvious substrate for the apical current sources induced by carbachol in the present study. Although the apical sources observed here can only be localized to the resolution allowed by the 150 μm interelectrode spacing used, their location is consistent with the apical interneuron projections described.

The dendrites of the apically directed interneurons are well situated to receive collaterals from pyramidal neurons, and it is reasonable to assume that the two collections of cells form a negative feedback circuit. Cycling activity would require tonic excitation of the pyramidal neurons. Cholinergic stimulation blocks potassium currents (Nakajima et al., 1986; Madison et al., 1987; Benson et al., 1988) and thereby causes slow depolarizations in hippocampal neurons (Benson et al., 1988). These depolarizations should result in pyramidal cell discharges as the apical inhibition initiated by the last round of firing dissipates. Field CA3 is densely interconnected by excitatory associational projections that, in the absence of inhibition, allow active pyramidal neurons to recruit their neighbors. This leads to synchronized EPSPs in the proximal dendritic regions innervated by the associational system and the appearance of current sinks in those regions. These events are the likely explanation for the ~10 msec sinks that precede the apical sources during carbachol-induced β activity. Taken together the results suggest that carbachol elicits β rhythms by enhancing (1) pyramidal cell spiking via direct (blocking potassium channels) and indirect (suppressing release from basket terminals) routes and (2) the responsivity of interneurons that receive pyramidal cell collaterals and project to the apical dendrites. Gradual dissipation of the IPSP would be accompanied by decreases in the extracellular current flow, the reappearance of pyramidal cell spiking, and the onset of a new cycle.

A key requirement of the above model is that spiking of pyramidal cells triggers a current source in the apical dendrites with temporal characteristics appropriate for the β wave. In accord with this, orthodromic activation of a pyramidal cell population caused highly damped β waves in the distal dendrites. The experiments involved adding a GABA receptor antagonist at concentrations that partially block IPSPs to reduce the inhibition that normally prevents pyramidal cell spiking. Under these conditions, responses with the polarity, distribution, and duration expected from collateral activation of apically directed GABAergic cells were obtained. Studies are now in progress to determine whether, as predicted, the apical current source is sensitive to cholinergic stimulation. The argument that carbachol-induced β is caused by the above-described feedback circuit also requires that the rhythm be blocked by antagonists of either AMPA or GABAa receptors. Both predictions were satisfied in the present study.

The above-described distribution of current sources responsible for β oscillations is suggestive of the types of local processing associated with the rhythm. GABA-mediated conductances in distal dendritic branches will markedly attenuate postsynaptic responses of pyramidal and granule cells to afferents from the entorhinal cortex while leaving those generated by associational inputs relatively intact. Assuming that the pertinent GABAergic cells have low thresholds, as do other interneurons in the hippocampus, activation of a small proportion of the pyramidal cell population would separate most of the population from extrinsic input for tens of milliseconds. The net effect of β (and possibly γ) would, according to this argument, be to impose temporal order on, or temporal requirements for, cortical activation of the hippocampus. Whether associational communication continues while the distal IPSP is imposed on the cell remains an open question. Pyramidal cell spiking that initiates the IPSP also sends excitatory input to other pyramidal cells along the extremely dense commissural–associational and Schaffer–commissural systems. The intrahippocampal projections also activate feedforward interneurons that both truncate the EPSPs and shunt further excitatory input. However, after having been activated, the feedforward interneurons enter a refractory period that reaches its maximum ~200 msec later (Mott and Lewis, 1991). Activation at the θ frequency (4–10 Hz) thus allows converging associational projections to circumvent the feedforward inhibitory system. Co-occurrence of θ and high-frequency rhythms could set up conditions such that the latter create brief windows during which intrinsic operations proceed in the absence of external inputs. Measuring the responses elicited by stimulation of associational fibers while the distal IPSP is present and the feedforward IPSP is refractory would provide some measure of the feasibility of this scenario.

Finally, it should be noted that although carbachol induced rhythmic activity in the β range in hippocampus, it triggered 40 Hz oscillations in the deep layers of the entorhinal cortex. Although this could be caused by damage of the connectivity between these structures in the slice [both θ and γ coherence between entorhinal cortex and hippocampus are relatively high *in vivo* (Charpak et al., 1995; Chrobak and Buzsaki, 1998)], the phenomenon was observed in a number of instances, and initial measurement suggests that the entorhinal γ and hippocampal β observed were in-phase. The distinction is not absolute in that 40 Hz activity was sometimes recorded from the hippocampus and was described in a previous study using carbachol (Fisahn et al., 1998). A recent experiment using tetanic stimulation to trigger oscillations in hippocampal slices found that transitions from the γ to the β range were accompanied by increases in the afterhyperpolarizing potentials (AHPs) that follow pyramidal cell spikes (Traub et al., 1999). AHPs have durations sufficient to account for the difference in the frequencies of the cholinergically induced rhythms. It should also be noted that diazepam sometimes caused a distinct 40 Hz component to be added to the carbachol-elicited activity. Diazepam should serve to enhance whatever degree of perisomatic inhibition remains after cholinergic suppression of GABA release and thus decrease the number of spikes emitted by the cells during the excitation phase of the rhythm. Reducing the number of spikes could eliminate the AHP and allow the membrane potential to return more quickly to firing threshold. It will be of interest in this regard to determine whether cholinergic agonists suppress evoked IPSPs in the entorhinal cortex to the same degree that they do in the hippocampus.

REFERENCES

Behrends JC, Bruggencate G (1993) Cholinergic modulation of synaptic inhibition in the guinea pig hippocampus in vitro: excitation of GABAergic interneurons and inhibition of GABA-release. J Neurophysiol 69:626–629.

Benson DM, Blitzer RD, Landau EM (1988) An analysis of the depolar-

ization produced in guinea pig hippocampus by cholinergic receptor stimulation. J Physiol (Lond) 404:479–496.
Boddeke HWGM, Best R, Boeijinga PH (1997) Synchronous 20 Hz rhythmic activity in hippocampal networks induced by activation of metabotropic glutamate receptors in vitro. Neuroscience 76:653–658.
Charpak S, Parae D, Llinas R (1995) The entorhinal cortex entrains fast CA1 hippocampal oscillations in the anaesthetized guinea-pig: role of the monosynaptic component of the perforant path. Eur J Neurosci 7:1548–1557.
Chrobak JJ, Buzsaki G (1998) Gamma oscillations in the entorhinal cortex of the freely behaving rat. J Neurosci 18:388–398.
Dickson CT, Alonso A (1997) Muscarinic induction of synchronous population activity in the entorhinal cortex. J Neurosci 17:6729–6744.
Fisahn A, Pike FG, Buhl EH, Paulsen O (1998) Cholinergic induction of network oscillations at 40 Hz in the hippocampus in vitro. Nature 394:186–189.
Freeman WJ (1975) Mass action in the nervous system. New York: Academic.
Frotscher M, Leranth C (1985) Cholinergic innervation of the rat hippocampus as revealed by choline acetyltransferase immunocytochemistry: a combined light and electron microscopic study. J Comp Neurol 239:237–246.
Gray CM, Singer W (1989) Stimulus-specific neuronal oscillation columns of cat visual cortex. Proc Natl Acad Sci USA 56:1698–1702.
Haberly L, Shepherd G (1973) Current density analysis of summed evoked potentials in opossum prepyriform cortex. J Neurophysiol 36:789–803.
Hajos N, Papp ECS, Acsady L, Levy A, Freund TF (1998) Distinct interneuron types express M2 muscarinic receptor immunoreactivity on their dendrites or axon terminals in the hippocampus. Neuroscience 82:355–376.
Howland B, Lettvin J, McCulloch W, Pitts W, Wall P (1955) Reflex inhibition by dorsal root interaction. J Neurophysiol 18:1–17.
Iijima T, Witter MP, Ichikawa M, Tominaga T, Kajiwara R, Matsumoto G (1996) Entorhinal-hippocampal interactions revealed by real-time imaging. Science 272:1176–1179.
Kay LM, Freeman WJ (1998) Bidirectional processing in the olfactory-limbic axis during olfactory behavior. Behav Neurosci 112:514–553.
Ketchum KL, Haberly LB (1993) Membrane currents evoked by afferent fiber stimulation in rat piriform cortex. I. Current source density analysis. J Neurophysiol 69:248–260.
Kolta A, Ambros-Ingerson J, Lynch G (1996) Early and late components of AMPA-receptor mediated field potentials in hippocampal slices. Brain Res 737:133–145.
Konopacki J, MacIver MB, Bland BH, Roth SH (1987) Carbachol-induced EEG "theta" activity in hippocampal brain slice. Brain Res 405:196–198.
Landfield PW, McGaugh JL, Tusa RJ (1972) Theta rhythm: a temporal correlate of memory storage processes in the rat. Science 175:87–89.
Larson J, Lynch G (1986) Induction of synaptic potentiation in hippocampus by patterned stimulation involves two events. Science 232:985–988.
Larson J, Wong D, Lynch G (1986) Patterned stimulation at the theta frequency is optimal for the induction of hippocampal long-term potentiation. Brain Res 368:347–350.
Larson J, Xiao P, Lynch G (1993) Reversal of LTP by theta frequency stimulation. Brain Res 600:97–102.
Leung LS (1985) Spectral analysis of hippocampal EEG in the freely moving rat: effects of centrally active drugs and relations to evoked potentials. Electroencephalogr Clin Neurophysiol 60:65–77.
Levey AI, Edmunds SM, Koliatsos V, Wiley RG, Helman CJ (1995) Expression of m1–m4 muscarinic acetylcholine receptor proteins in rat hippocampus and regulation by cholinergic innervation. J Neurosci 15:4077–4092.
Lewis PR, Shute CCD (1967) The cholinergic limbic system: projections to hippocampal formation, medial cortex, nuclei of the ascending cholinergic reticular system, and the subfornical organ and supra-optic crest. Brain 90:521–540.
Lynch G, Rose G, Gall C (1978) Anatomical and functional aspects of the septo-hippocampal projections. In: Functions of the septo-hippocampal system, Ciba foundation symposium 58, pp 5–24. Amsterdam: Elsevier.
MacVicar BA, Tse FWY (1989) Local neuronal circuitry underlying cholinergic rhythmical slow activity in CA3 area of rat hippocampus. J Physiol (Lond) 417:197–212.
Madison DV, Lancaster B, Nicoll RA (1987) Voltage-clamp analysis of cholinergic action in the hippocampus. J Neurosci 7:733–741.
Matthews DA, Salvaterra PM, Crawford GD, Houser CR, Vaughn JE (1987) An immunocytochemical study of choline acetyltransferase-containing neurons and axon terminals in normal and partially deafferented hippocampal formation. Brain Res 402:30–43.
Mitzdorf U (1985) Current source-density method and application in cat cerebral cortex: investigation of evoked potentials and EEG phenomena. Physiol Rev 65:37–100.
Mosko S, Lynch G, Cotman CW (1973) Distribution of the septal projections to the hippocampus of the rat. J Comp Neurol 152:163–174.
Mott DD, Lewis DV (1991) Facilitation of the induction of long-term potentiation by GABAB receptors. Science 252:1718–1720.
Nakajima Y, Nakajima S, Leonard RJ, Yamaguchi K (1986) Acetylcholine raises excitability by inhibiting the fast transient potassium current in cultured hippocampal neurons. Proc Natl Acad Sci USA 83:3022–3026.
Nicholson C (1973) Theoretical analysis of field potentials in anisotropic ensembles of neuronal elements. IEEE Trans Biomed Eng 20:278–288.
Nicholson C, Freeman J (1975) Theory of current source-density analysis and determination of conductivity tensor for anuran cerebellum. J Neurophysiol 38:356–368.
Nicholson C, Llinas R (1975) Real time current source density analysis using multi-electrode array in cat cerebellum. Brain Res 100:418–424.
Oka H, Shimono K, Ogawa R, Sugihara H, Taketani M (1999) A new planar multielectrode array for extracellular recording: application to hippocampal acute slice. J Neurosci Methods 93:61–67.
Pitler TA, Alger BE (1992) Cholinergic excitation of GABAergic interneurons in the rat hippocampal slice. J Physiol (Lond) 450:127–142.
Singer W (1998) Consciousness and structure of neuronal representations. Philos Trans R Soc Lond B Biol Sci 353:1829–1840.
Stumpf C (1965) Drug action on the electrical activity of the hippocampus. Int Rev Neurosci 8:77–138.
Traub RD, Spruston N, Soltesz I, Konnerth A (1998) Gamma-frequency oscillations: a neuronal population phenomenon, regulated by synaptic and intrinsic cellular processes, and inducing synaptic plasticity. Prog Neurobiol 55:563–575.
Traub RD, Whittington MA, Buhl EH, Jefferys JGR, Faulkner HJ (1999) On the mechanism of the γ→β frequency shift in neuronal oscillations induced in rat hippocampal slices by tetanic stimulation. J Neurosci 19:1088–1105.
van der Linden S, Panzica F, de Curtis M (1999) Carbachol induces fast oscillations in the medial but not in the lateral entorhinal cortex of the isolated guinea pig brain. J Neurophysiol 82:2441–2450.
Vanderwolf CH (1969) Hippocampal electrical activity and voluntary movement in the rat. Electroencephalogr Clin Neurophysiol 26:407–418.
Vertes RP, Kocsis B (1997) Brainstem-dienchephalo-septhippocampal systems controlling the theta rhythm of the hippocampus. Neuroscience 81:893–926.
Williams JH, Kauer JA (1997) Properties of carbachol-induced oscillatory activity in rat hippocampus. J Neurophysiol 78:2631–2640.